Chemical Methodologies

Journal homepage: http://chemmethod.com

Original Research Article

Synthesis and Structural Analysis of a Novel Stable Quinoline Dicarbamic Acid: X-Ray Single Crystal Structure of (2-((4-((2-(Carboxy(methyl)amino)ethoxy)carbonyl) quinoline-2-yl)oxy) ethyl) (methyl)-carbamic Acid and Molecular Docking Assessments to Test Its Inhibitory Potential against SARS-CoV-2 Main Protease

Ahmed Selmi[1,*], Armin Zarei[2], Wafa Tachoua[3], Horst Puschmann[4], Hakimeh Teymourinia[2,5,6], Ali Ramazani[2,5,*]

[1]*Laboratory of Physico-Chemistry of Materials, Faculty of Sciences of Monastir, 5019 Monastir, Tunisia*
[2]*Department of Chemistry, Faculty of Science, University of Zanjan, Zanjan 45371-38791, Iran*
[3]*Nature and Life Sciences Department, Benyoucef Benkhedda University, Didouche Mourad, 16000, Algiers, Algeria*
[4]*OlexSys Ltd, Durham University, South Road, Durham, DH1 3LE, UK*
[5]*Department of Biotechnology, Research Institute of Modern Biological Techniques (RIMBT), University of Zanjan, Zanjan 45371-38791, Iran*
[6]*Trita Nanomedicine Research Center (TNRC), Zanjan Health Technology Park, Postal code 45156-13191, Zanjan, Iran*

ARTICLE INFO

Article history

Submitted: 2022-03-27
Revised: 2022-04-03
Accepted: 2022-04-17
Manuscript ID: CHEMM-2203-1462
Checked for Plagiarism: **Yes**
Language Editor:
Dr. Behrouz Jamalvandi
Editor who approved publication:
Dr. Mohsen Oftadeh

DOI:10.22034/CHEMM.2022.335353.1462

KEYWORDS

Crystal structure
Single X-ray crystal structure
COVID-19
SARS-CoV-2 main protease
Molecular docking

ABSTRACT

The crystal structure of quinoline derivative with empirical formula ($C_{18}H_{21}N_3O_7$) was determined using single crystal X-ray diffraction, which belongs to the monoclinic system with the $P2_1/c$ space group. The cohesion and stabilization of the structure were provided by C-H...O hydrogen bond and Van-Der Waals interactions. A molecular docking study was performed to determine its antiviral potency between the SARS-CoV-2 main protease (M^{pro}) (PDB ID: 6Y2E) and chloroquine was chosen as a standard because of its similarity with our synthetic quinoline-based compound. Six herbal compounds and synthetic drugs bound to the active site of the target in order to compare their results with synthetic quinoline-based compound. This synthetic compound showed the lowest binding energy of -7.6 kcal.mol^{-1}, proving that this molecule seems to be a good candidate against the SARS-CoV-2.

* Corresponding author: Ali Ramazani
✉ E-mail: aliramazani@gmail.com

GRAPHICAL ABSTRACT

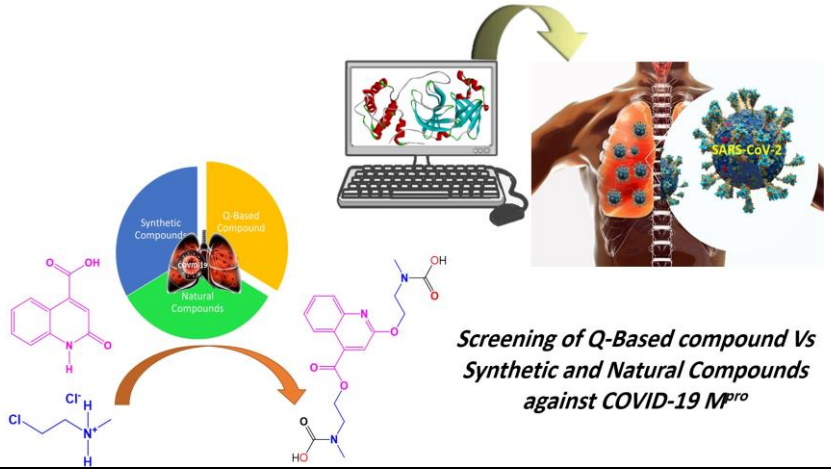

Introduction

The recent fatal widespread of coronavirus disease 2019 (COVID-19) influenced all strolls of life, cleared out the world in lockdown, and tainted millions of individuals around the globe [1, 2]. Severe Acute Respiratory Corona Virus-2 (SARS-CoV-2) as a potentially transmissible serious acute respiratory infection caused a pandemic in 2019 [3-5]. According to the World Health Organization (WHO), two out of the ten people infected with SARS-CoV-2 seems to experience severe forms of the disease [6]. Individuals with morbidity, such as those with chronic diseases such as cardiovascular disease, pulmonary disease, diabetes or cancer, among others, are at greater risk of developing severe forms of the disease [7]. From early months of the outbreak, preventive policies including quarantine, social distancing, etc. were adopted to prevent the further spread of the pandemic whole around the globe, which dearly influenced the global economy [8]. From genetic sequence point of view, SARS-CoV-2 is a positive-sense single-stranded RNA virus that belongs to beta-coronavirus family, assumed to be around 80% similar to MERS and SARS [9]. This novel type of coronavirus comprises various proteins like envelope (E), spike (S), membrane (M), and nucleocapsid (N). The spike glycoproteins also exist on the surface of SARS-CoV-2 encompassing two subunits (S1 and S2), by which they can attach to the host cell namely ACE-2 (Angiotensin converting enzyme 2) for facilitation of a cell fusion process [10]. It deserves to be pointed out that as far as cell fusion and cell entry procedures were accomplished, polypeptides would be prepared through genome transcription of the SARS-CoV-2. These polypeptides would be proteolytically cleaved using proteases (3CLpro, and PLpro) for different proteins fabrication [11]. Hence, main protease (M^{pro}) enzyme plays a significant role in proteolytically cleavage in SARS-CoV-2 and prepares considerable proteins for viral replication [12]. Targeting this vital protein can be the best candidate for therapeutic repositioning. Over the last two years, SARS-CoV-2 outbreak has been a great challenge for research groups entire the world and they are still struggling to find suitable antiviral drugs to tackle the present crisis. Therefore, a wide-range of naturally occurring compounds and new synthetic components have been expanded and tested against the viral disease [13-15]. Although various types of vaccines hit the market and a couple of billions globally got vaccinated, the death rate has not become zero and people still die because no promising antiviral licensed drugs against SARS-CoV-2 exists yet. Recent advances in information technology have made it possible to considerably limit the search time and has opened a new horizon to discovery novel drugs using bioinformatics tools such as "Molecular Docking" and "Molecular screening and scoring", which enabled us to predict and calculate the position and interactions between ligand (drug) and target (usually protein) [16]. Therapeutic repositioning of synthetic and naturally occurring compounds with suitable biological peculiarities against viral diseases have aroused much attention because it

is a time-saving process. Of heterocyclic compounds, quinoline is an advantageous chemical structure that appears as a remarkable assembly motif for the improvement of new drug entities, which provides high biological features such as anti-inflammatory, cardiovascular, antifungal, antimalarial, antibacterial, and anticancer effects [17]. Zhao *et al*. shed light on the potential of quinoline and quinazoline derivatives against SARS-CoV-2 RdRp, showing fascinating antiviral inhibition along with low cytotoxicity [18]. Another study has also delineated the great antiviral performance of quinoline derivatives (chloroquine and hydroxychloroquine) against viral targets of SARS-CoV-2 in which hydroxychloroquine had a supreme potential due to making H-bond with amino acid moiety of the target [19]. So, the highly antiviral potential of quinoline entities has inspired us to develop a novel quinoline-based compound to in silico test its affinity against SARS-CoV-2 M^{pro} using molecular docking tools. We have presented a novel and simple route to successful synthesis of the quinoline-based compound, which was then subjected to X-ray diffraction. Next, its antiviral potency against SARS-CoV-2 Mpro was tested using Autodock Vina in order to compare its antiviral performance with various synthetic drugs (Favipiravir, oseltamivir, ribavirin), compounds from natural sources (curcumin, piperin, capsaicin) as well as chloroquine as a standard (Supplementary materials TABLE S1).

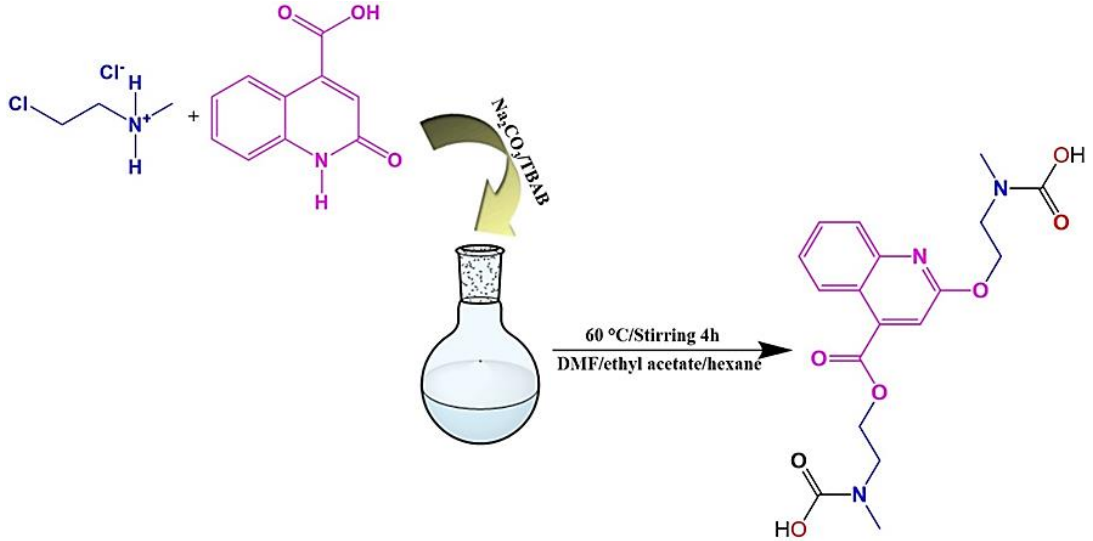

Figure 1: Synthesis of (2-((4-((2-(carboxy(methyl)amino)ethoxy)carbonyl)quinoline-2-yl)oxy)ethyl)(methyl)-carbamic acid

Materials and Methods

All the initial materials needed for the synthesis of Q-based derivative were purchased from Merck, Sigma-Aldrich, and Flucka companies. FTIR spectra were performed on a Shimadzu FT-IR-8400 spectrophotometer by the transmission method using the potassium bromide pellet.

Synthesis of (2-((4-((2-(carboxy (methyl) amino) ethoxy) carbonyl) quinoline-2-yl) oxy) ethyl) (methyl)-carbamic acid

Initially, 0.8 g (4.23 mmol) of 2-oxo-1, 2-dihydro-quinoline-4-carboxylic acid mixed with the solution comprising 0.75 g (4.23 mmol) of 2-chloro-*N*-ethy-1-methylaminium chloride, 1.16 g (8.46 mmol) of Na_2CO_3 and 0.13 g (0.423 mmol) of tetra-*n*-butyl ammonium bromide (TBAB), and resulting mixture was then added to a solution composed of 0.8 g (4.23 mmol) of 2-oxo-1,2-dihydroquinoline-4-carboxylic acid, followed by stirring and heating up to 60 °C for 4 h in a mixture of DMF/ethyl acetate/hexane (10% / 20% / 70%). The obtained precipitate was filtered off and then dissolved in ethanol, and after three days, the colorless single crystals were gained by slow evaporation (Supplementary Materials Scheme S1).

Single Crystal X-ray diffraction of (2-((4-((2-(carboxy (methyl) amino) ethoxy) carbonyl) quinoline-2-yl) oxy) ethyl) (methyl)-carbamic acid

Colorless Single crystal of the prepared compound were selected and mounted in on an APEX II

diffractometer. The crystal was kept at 293.15 K during data collection. The structure was solved by the olex2 [20] using Charge Flipping and refined with the SHELXL [21] refinement package using full matrix least squares minimization on F2. All atoms were refined anisotropically except for hydrogen atoms, which were fixed geometrically to their carrier atoms. The final R_1 was 0.0366 (I > 2σ (I)) and wR_2 was 0.1215.

Infrared Spectrum of (2-((4-((2-(carboxy (methyl) amino) ethoxy) carbonyl) quinoline-2-yl) oxy) ethyl) (methyl)-carbamic acid

Sample crystals were mixed with dispersed KBr powder (with 1:100 molar ratio). Then, the mixture was pressed using hydraulique press into a disc within approximately 3 mm of thickness, and spectrum was recorded in wave number range between 4000 and 400 cm^{-1}.

Molecular docking study

Preparation of receptor and ligands

The unliganded crystal structure of SARS-CoV-2 M^{pro} (ID: 6Y2E) at a resolution of 1.75 Å [12] was downloaded from the PDB (https://www.rcsb.org) [13]. This viral protease has a molecular weight of 33.79 kDa as determined by mass spectrometry. It is a homodimer, where each monomer comprises three structural domains; domain I (8-101 aa) with II (102-184 aa) adopting an antiparallel β barrel topology. However, domain III (201-301) contains five α-helices arranged into a largely antiparallel globular cluster, connected to domain II by means of a long loop region. Unlike cysteine proteases whose active site hosts three catalytic residues (His, Cys and Asn), the active site of M^{pro} lacks the third residue, containing a catalytic dyad comprising two amino acids (His41, Cys145) located among domain I and II (Figure 2).

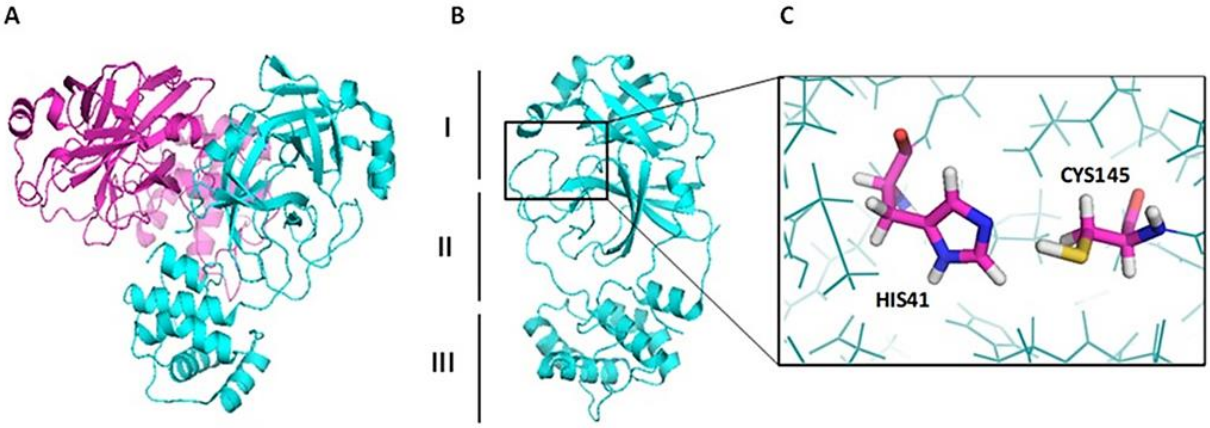

Figure 2: (A) Cartoon representation of the dimeric structure of Mpro. (B) The three domains of the Mpro designated by Roman numerals. (C) Stick representation of the catalytic dyad of Mpro formed by Cys41 and His145 residues

As for synthetic quinoline-based compound, its gained crystal structure from X-ray Diffraction in cif format optimized and converted to sdf using gaussian (V.09). Structures of herbal compounds (curcumin, piperin, capsaicin) along with synthetic drugs (favipiravir, oseltamivir, ribavirin) in SDF format were downloaded from Pubchem database. Our quinoline-based compound as well as other synthetic and herbal ligands in sdf format were converted to PDB using Open Babel, by which input files were systematically calculated in vasuo free energy and determination of conformers led to retrieval of conformers with the lowest energy in order to reduce the input files [22, 23]. Moreover, all of pre-processing steps according to previous researches were fulfilled via Autodock Tools (ADT) (1.5.6) [24]. The polar hydrogens, gastiger charges along with atom types of whole ligands and receptor were added through the ADT. As for ligands, all torsions were set as active owing to perform searching phase space. Residues were kept rigid with the exception of His 41 and Cys 145 [25].

Molecular docking using Autodock Vina

Molecular docking was conducted using Vina 1.1.2 on Windows 10 platform (64-bit) with Lenovo IdeaPad L340-15IWL (CORE i7, system memory: 256 GB SSD, 12 GB RAM). The grid box dimension

set on 32 × 32 × 32 cubic angstroms with a grid spacing of 1.0 angstrom [26]. The other parameters remained as default. The synthetic quinoline-based compound was flexibly docked with our target by Autodock Vina for comparing its binding affinity with those of herbal and synthetic drugs against SARS-CoV-2 M^{pro}. Visualization of results were gained using Discovery studio 4.5.

Results and Discussion

(2-((4-((2-(carboxy (methyl) amino) ethoxy) carbonyl) quinoline-2-yl) oxy) ethyl) (methyl)-carbamic acid was simply prepared from commercially available materials. The structure of Q-based compound was confirmed by FTIR spectrum (Figure 3). Vibrational spectrum of this compound was shown in the region of infrared a wide band referring to stretch vibrations of the group OH at 3132 cm^{-1}, suggesting solid state hydrogen bond. The deformation of the hydroxy (OH) group was observed near 1470 and 897 cm^{-1} [27]. The C−N and C-O stretch vibrations were observed at 1286 and 1206 cm^{-1}, respectively, while the C=N stretch deformation was situated at 1576 cm^{-1}. In the vibrational spectrum, the vibration band referring to the C=N stretch of the pyridine was displaced by 1542 cm^{-1} [28]. The peaks at 1725 and 1665 cm^{-1} demonstrated carboxyl and amid groups. Absorption bands at 3317, 2926 and 1647 were imputed to the stretching vibration of O-H, C-H and C=C, respectively. In addition, the peaks at 1615 and 1450 cm^{-1} can be the result of skeletal vibration of aromatic ring [29]. The stretching band OH, around 3100 cm^{-1}, the band referring to the stretching of the carboxylic group ν(COOH).

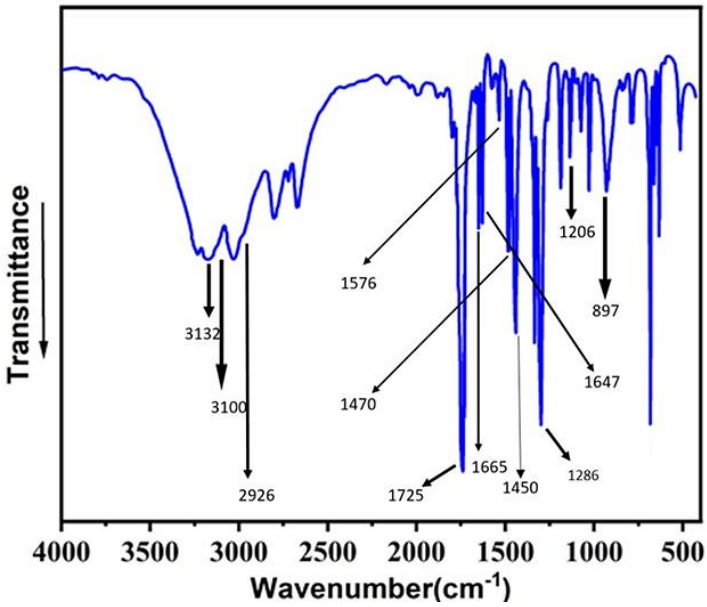

Figure 3: Infrared spectrum showing the absorption bands of the different entities of the synthetic quinoline-based compound

A suitable colorless crystal with dimensions 0.17 × 0.13 × 0.11 mm3 was selected and glued on a glass fibre and mounted on APEX II diffractometer operating with Mo (Kα) = 0.71073 A°. The structure was solved using 4350 independent reflections and the structure was solved using olex2 solution program [30]. The model was refined with ShelXL [31] by using full matrix least squares minimization on F^2. All non-hydrogen atoms were refined anisotropically. Hydrogen atoms positions were calculated geometrically and refined using riding model [20]. The convergence of the structure was obtained for the final convergence of the structure when the final WR and R would be 0.1215 and 0.0366 (I≥2σ(I)), respectively. The crystal data and structure refinement results are summarized in Supplementary materials Table S2 and ORTEP view showing the atomic labeling scheme, with thermal ellipsoids drawn at 50% probability levels shown in Figure 4.

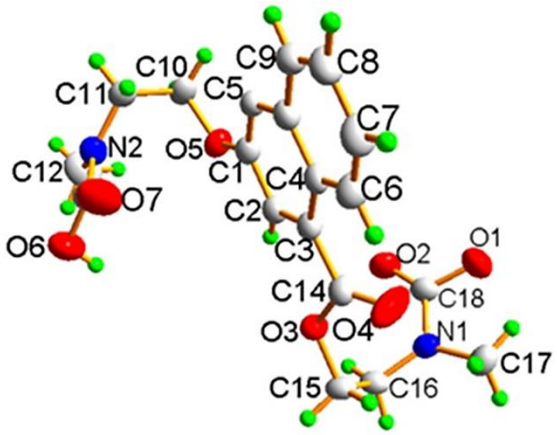

Figure 4: Ortep plot at 50% probability levels of the assymetric unit of the structure

The molecular stability of the crystal is ensured by almost strong intra and intermolecular hydrogen bonds of the C-H...O type. The Donor-Acceptor distances are between 1.79 and 2.57 Å, while the angles are in the range of 113.5 to 133º. The present hydrogen bonds in the crystalline cohesion of the compound are mentioned in Table 1.

Table 1: Principal hydrogen bonds distances (Å) and angles (°) inside the crystal cell

D-H...A	d(D-H)/Å	d(H-A)/Å	d(D-A)/Å	D-H-A/°
C11-H11B...O8[1]	0.97	2.56	3.2640(14)	129.1
C16-H16A...O2[2]	0.97	2.57	3.2180(13)	124.6
C17-H17A...O1	0.96	1.81	2.3578(15)	113.3
C17-H17C...O4	0.96	2.54	3.2767(16)	133.2
C12-H12B...O7	0.96	1.80	2.3551(18)	113.9
Symmetry code: (i)1-1+x,+y,+z; (ii) 1+x,+y,+z				

Within the quinoline derivative molecule, the C-C distances belonging to the benzene ring are moderately 1.41Å, while the C-C(N)-C angles range between 116.62(9) and 122.06(9)º. In the COOH carboxylate terminal group, the distances C-O and C=O are 1.2108(15), and 1.3570(15) Å respectively (**TABLE 2, 3**) [9]. **Table 3** represents the main distances and angles of the synthetic compound. Another point that should be reported about the flexibility of the terminal groups makes it reactive in biological reactions.

Table 2: Interatomic distances (Å) for shortest contact between atoms of the compound

A-B	Distance(Å)	A-B	Distance(Å)
O3-C14	1.3384(12)	C3-C4	1.4398(13)
O3-C15	1.4540(12)	C3-C14	1.4985(14)
O6-C1	1.3510(12)	O7-C13	1.3570(15)
O6-C10	1.4432(12)	O8-C13	1.2108(15)
N3-C1	1.2995(14)	O4-C14	1.1994(14)
N3-C5	1.3808(14)	C2-C1	1.4246(14)
N2-C11	1.4478(14)	C4-C5	1.4179(15)
N2-C13	1.3366(14)	C4-C6	1.4139(15)
N2-C12	1.4364(14)	C11-C10	1.5218(15)
O2-C18	1.2108(14)	C5-C9	1.4167(14)
O1-C18	1.3551(13)	C6-C7	1.3723(16)
N1-C18	1.3481(13)	C9-C8	1.3562(18)
N1-C16	1.4449(14)	C8-C7	1.4031(19)
N1-C17	1.4551(13)	C16-C15	1.5095(15)
C3-C2	1.3587(14)		

Table 3: Bond Angles (°) between adjacent atoms of the compound

A-B-C	Angle(°)	A-B-C	Angle(°)
C14-O3-C15	118.17(8)	O4- C14- O3	123.82(10)
C1-O6 -C10	117.96(8)	O4- C14- C3	124.95(10)
C1- N3- C5	116.76(9)	N2- C11- C10	111.98(9)
C13-N2 -C11	122.15(9)	O2- C18- O1	122.01(10)
C13- N2- C12	112.69(10)	O2- C18- N1	128.05(10)
C12- N2 -C11	123.39(10)	N1- C18- O1	109.95(9)
C18- N1 -C16	122.33(9)	N3- C5- C4	123.45(9)
C2 -C3- C4	111.72(9)	N3- C5- C9	117.33(10)
C18- N1- C17	123.61(9)	C9- C5- C4	119.19(10)
C16- N1- C17	119.21(9)	N2- C13- O7	109.80(10)
C2- C3- C14	118.72(9)	O8- C13- N2	128.08(11)
C4- C3- C14	122.06(9)	O8- C13- O7	122.12(11)
C3- C2- C1	118.79(9)	C7- C6- C4	120.51(11)
O6- C1- C2	114.05(9)	C8- C9- C5	120.73(11)
N3- C1- O6	120.91(9)	C9- C8- C7	120.41(10)
N3- C1- C2	125.03(9)	O-6 C10- C11	110.31(8)
C5- C4- C3	116.62(9)	N1- C16- C15	113.38(9)
C6- C4- C3	124.75(10)	C6- C7- C8	120.51(11)
C6- C4- C5	118.62(9)	O3- C15- C16	109.91(8)
O3- C14- C3	111.19(8)		

Molecular docking results

Molecular docking is depicted as an effective strategy to examine the interactions between ligand and the binding pose of proteins [32, 33]. Here, Autodock Vina was utilized to explore the antiviral affinity of synthetic quinoline-based compound against SARS-CoV-2 M^{pro} and compare it with those of naturally occurring and synthetic drugs. Our synthetic quinoline derivative component and herbal compounds as well as synthetic drugs were flexibly docked to the binding pocket of viral protease. Quinoline derivatives possessed antiviral potency *e.g*., Loesgen; a group of quinoline-based components were synthesized and their antiviral potential against HIV-1 was checked out, demonstrating that quinoline analogous effectively bound to HIV-1 reverse transcriptase, inhibiting RNase H activity [34]. In addition, two chemical compounds based on quinoline scaffold have been recently synthesized with potential biological active agents to test their antiviral potency versus dengue virus serotype 2, postulating dose-dependent inhibition against the virsus with the ability to ruin accumulation of the viral envelope glycoprotein in the infected cells [35].

Visual screening of 4 compounds with the lowest binding energies is illustrated in Figure 5. As can be seen in Table 4, our fabricated quinoline derivative (-7.6 kcal/mol) (compound **a**) exhibited a remarkable binding energy even comparable to those of synthetic and herbal structures. As shown in Figure 5a, compound **a** attached to viral receptor through 5 H-bonds with SER 46, ASN 142, GLU 166 amino acid residues and its phenyl ring demonstrated 2 π-alkyl hydrophobic interactions with MET 49, MET 165, and most importantly, it could block CYS 145 (one of the M^{pro}'s active residue) through π-alkyl interaction. Taking the meaningful antiviral potency of quinoline derivatives, compound **a** demonstrated the lowest binding energy (having energy difference of 1-2 Kcal/mol in average with synthetic drugs), 5 H-bonds as well as blocking Cys 145; as its merit, it may be the potential nomination to inhibit SARS-CoV-2 M^{pro} and might be on the call for further *in vitro* and *in vivo* investigation to prove their antiviral potential.

Table 4: Interactions and binding scores of quinoline-based compound with M^{pro} in comparison to those of herbal and synthetic compounds

Mark.	Compound	Binding Energy (Kcal/mol)	Interacting amino acid residues	No. of hydrogen bonds	Hydrogen bond interaction
f	Chloroquine$^{\alpha}$	-6.0	HIS 41, CYS 44, MET 49, ASN 142, GLY 143, CYS 145	1	GLY 143
a	Quinole derivative$^{\beta}$	-7.6	SER 46, MET 49, PHE 140, LEU 141, ASN 142, CYS 145, MET 165, GLU 166	5	SER 46, ASN 142, GLU 166
b	Curcumin$^{\gamma}$	-7.3	MET 49, PHE 140, GLY 143, SER 144, CYS 145	3	GLY 143, SER 144
c	Piperin$^{\gamma}$	-6.9	THR 24, THR 25, MET 165, GLU 166	2	THR 25, GLU 166
e	Capsaicin$^{\gamma}$	-6.2	HIS 41, MET 49, LEU 141, ASN 142, CYS 145, HIS 164	2	ASN 142, HIS 164
h	Favipiravir$^{\Delta}$	-5.4	PHE 140, ASN 142, GLY 143, CYS 145, MET 165, GLU 166	3	PHE 140, GLY 143, GLU 166
g	Oseltamivir$^{\Delta}$	-5.9	HIS 41, ASN 142, CYS 145, GLU 163, GLU 166, GLN 189	3	ASN 142, GLU 166, GLN 189
d	Ribavirin$^{\Delta}$	-6.7	HIS 41, ASN 142, GLY 143, LEU 141, CYS 145, HIS 163, GLU 166	5	ASN 142, GLY 143, LEU 141, HIS 163, GLU 166

Control compound: α, Synthetic Quinoline compound: β, Extracted from plant sources: γ, Synthetic drug: Δ.

There is a similarity between the structure of chloroquine (compound **f**) and compound **a**, so it was selected as a standard to compare its antiviral potential against SARS-CoV-2 M^{pro}. Compound **f** attached to active site of M^{pro} with binding energy of -6.0 kcal/mol (around 1.6 lower than that of compound **a**), and bore just one H-bond with GLY 143, authenticating the fact that compound **a** has a stronger antiviral potency even compared with the standard compound (Figure 5d). Among compounds from plants and synthetic sources, curcumin (compound **b**) has ranked second in terms of binding energy (-7.3), after which Piperin (compound **c**) showed up itself as the other potential inhibitor against SARS-CoV-2 M^{pro} (-6.9). Curcumin (compound **b**), the essential curcuminoind compound existing in turmeric spice, has exhibited a wide range of biological activities like antimicrobial agent, restraining the replication of numerous various types of fungi, bacteria and viruses [36]. This naturally occurring compound ranked second in terms of binding affinity, and bound to the viral target through 3 H-bonds (with GLY 143, SER 144) along with making π-alkyl with MET 49 and CYS 145 (Figure 5b), strengthening its inhibitory effect against the virus, but lesser than compound **a**. Compound **c** is also an alkaloid found in black pepper and some other sort of peppers, representing anti-inflammatory, anti-allergic, neuroprotective [37] anticancer properties [38], showing a binding energy of -6.9 kcal/mol. Compound **c** appeared as 2 H-bonding with THR 25, GLU 166 as well as one hydrophobic interaction by which its structure may be fortified (Figure 5c). Capsaicin (compound **e**) as a common dietary supplement exists in chili pepper, revealing a significant antiviral potential against Lassa virus entry (with EC50 of 6.9-10.0 μmol/L) [39]. This natural compound delineated a binding energy -6.2 Kcal/mol and bound to viral target via ASN 142 and HIS 164 (Supplementary materials Figure S2d). Interestingly, the other three synthetic drugs such as ribavirin (compound **d**), an antiviral pharmaceutical utilized for oral and inhaled treatment for RSV (Respiratory Syncytial Virus) Infection [40] and hepatitis C [41], oseltamivir (compound **g**), known as an antiviral medicine used against influenza A and B [42, 43], and favipiravir (compound **h**), known as an anti-influenza medication against RNA infectious virus [44], showed much lower binding affinities than that of compound **a**, -6.7, -5.9 and -5.4, respectively.

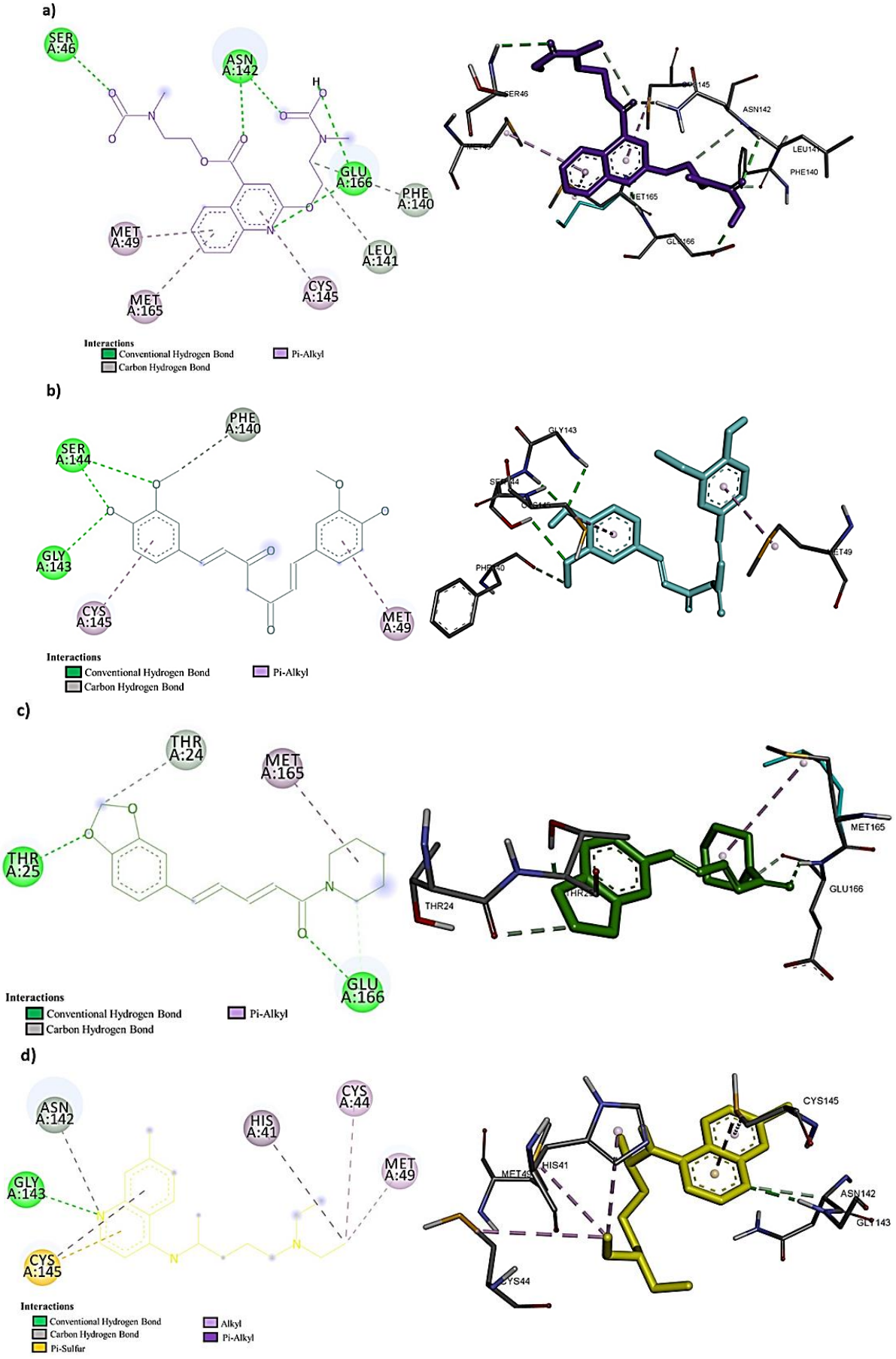

Figure 5: 2D and 3D interactions between **a)** Quinoline-derivative **b)** Curcumin **c)** Piperin **d)** Chloroquine and active site of SARS-CoV-2 Mpro

As illustrated in Supplementary materials Figure S2a, compound **d** delineated higher number of hydrogen bonds (5) (with PHE 140, LEU 141, GLY 143 and GLU 166) among three tested synthetic drugs and equals compound **a**. However, compounds **g** and **h** showed equal number of H-bonds (3) with the viral receptor. Although compound **d** and **h** could block CYS 145 through one π-sulfur interaction, compound **g** represented higher blocking affinity due to making electrostatic interactions not only with CYS 145, but also with HIS 41 (Supplementary materials Figure S2b, c). As The relative energy difference between compound **a,** especially with these three synthetic drugs, making more electrostatic interactions and 5 H-bonds reinforces the hypothesis of its high potential antiviral activity against SARS-CoV-2 M^{pro}.

Conclusion

In the present study, a novel quinoline derivative compound with empirical formula ($C_{18}H_{21}N_3O_7$) was synthesized through a facile technique, which its single crystal structure was prepared using XRD. Then, its antiviral performance against SARS-CoV-2 M^{pro} was conducted via autodock Vina to test its inhibitory effects compared with those of herbal (Curcumin, Piperine, Capsaicin), and synthetic compounds (Favipiravir, Oseltamivir, Ribavirin). Chloroquine was also used as positive control. Interestingly, concerning the molecular docking results, quinoline-based compound represented the lowest binding affinity of -7.6 kcal/mol even compared with those of synthetic drugs. Another criterion for showing antiviral potential of our synthetic compound is the number of Hydrogen bonds; this quinoline-based compound delineated more Hydrogen bonds among all tested ligands, bolding the point that it can be a promising nomination versus SARS-CoV-2 if further *in vitro* and *in vivo* will check out its antiviral potential.

Acknowledgments

We highly appreciate Dr. Abdelkader Ayoub, professor emeritus of pneumology and allergology at the Faculty of Sciences of Sfax, Tunisia, for his help.

Funding

This research did not receive any specific grant from fundig agencies in the public, commercial, or not-for-profit sectors.

Authors' contributions

All authors contributed toward data analysis, drafting and revising the paper and agreed to responsible for all the aspects of this work.

Conflict of Interest

We have no conflicts of interest to disclose.

ORCID

Ali Ramazani

https://www.orcid.org/0000-0003-3072-7924

References

[1]. Lu R., Zhao X., Li J., Niu P., Yang B., Wu H., Wang W., Song H., Huang B., Zhu N., Bi Y., Ma X., Zhan F., Wang L., Hu T., Zhou H., Hu Z., Zhou W., Zhao L., Chen J., Meng Y., Wang J., Lin Y., Yuan J., Xie Z., Ma J., Liu W.J., Wang D., Xu W., Holmes E.C., DPhil G.F.G., Wu G., Chen W., Shi W., Tan W., *Lancet*, 2020, **395**:565 [Crossref], [Google Scholar], [Publisher]

[2]. Tabarsi P., Vahidi H., Saffaei A., Hashemian S.M.R., Jammati H., Daraei B., Mahboubi A., Kobarfard F., Marjani M., Moniri A., Abtahian Z., Abedini A., Eslaminejad A., Heshmatnia J., Mirenayat M.S., Fakharian A., Seifi S., Sadeghi M., Dastan A., Haseli S., Nadji S.A., Eskandari R., Yousefian S., Varahram M., Zali A., Velayati A.A., Dastan F., *Iran. J. Pharm. Res.*, 2021, **20**:1 [Crossref], [Google Scholar], [Publisher]

[3]. Mehraeen E., Karimi A., Barzegary A., Vahedi F., Afsahi A.M., Dadras O., Moradmand-Badie B., Alinaghig S.A.S., Jahanfar S., *Eur. J. Integr. Med.*, 2020, **40**:101226 [Crossref], [Google Scholar], [Publisher]

[4]. Zarei A., *Nat. Prod. Res.*, 2021, 1 [Crossref], [Google Scholar], [Publisher]

[5]. Zarei A., Fardood S.T., Moradnia F., Ramazani A., *Eurasian Chem. Commun.,* 2020, **2**:798 [Crossref], [Google Scholar], [Publisher]

[6]. Jin Y., Ji W., Yang H., Chen S., Zhang W., Duan G., *Sig. Transduct. Target. Ther.*, 2020, **5**:1 [Crossref], [Google Scholar], [Publisher]
[7]. Laxminarayan R., Vinay T.G., Kumar K.A., Wahl B., Lewnard J.A., *Lancet Infect. Dis.*, 2021, **21**:1665 [Crossref], [Google Scholar], [Publisher]
[8]. Bates A.E., Mangubhai S., Milanés C.B., Rodgers K.U., Vergara V., *Nat. Commun.*, 2021, **12**:1-4 [Crossref], [Google Scholar], [Publisher]
[9]. Geller C., Varbanov M., Duval R.E., *Viruses*, 2012, **4**:3044 [Crossref], [Google Scholar], [Publisher]
[10]. Walls A.C., Park Y.J., Tortorici M.A., Wall A., McGuire A.T., Veesler D., *Cell*, 2020, **181**:281 [Crossref], [Google Scholar], [Publisher]
[11]. Anand K., Ziebuhr J., Wadhwani P., Mesters J.R., Hilgenfeld R., *Science*, 2003, **300**:1763 [Crossref], [Google Scholar], [Publisher]
[12]. Vuong W., Khan M.B., Fischer C., Arutyunova E., Lamer T., Shields J., Saffran H.A., McKay R.T., van Belkum M.J., Joyce M.A., Young H.S., Tyrrell D.L., Vederas J.C., Lemieux M.J., *Nat. Commun.*, 2020, **11**:1 [Crossref], [Google Scholar], [Publisher]
[13]. Hussain S., Alsinai A., Afzal D., Maqbool A., Afzal F., Cancan M., *Chem. Methodol.*, 2021, **5**:485 [Crossref], [Google Scholar], [Publisher]
[14]. Touret, F., de Lamballerie X., *Antivir. Res.*, 2020, **177**:104762 [Crossref], [Google Scholar], [Publisher]
[15]. Wu C.C., Fang C.Y., Hsu H.Y., Chen Y.J., Chou S.P., Huang S.Y., Cheng Y.J., Lin S.F., Chang Y., Tsai C.H., Chen J.Y., *Antivir. Res.*, 2016, **132**:99 [Crossref], [Google Scholar], [Publisher]
[16]. Onawole A.T., Sulaiman K.O., Kolapo T.U., Akinde F.O., Adegoke R.O., *Virus Res.*, 2020, **285**:198022 [Crossref], [Google Scholar], [Publisher]
[17]. Matada B.S., Pattanashettar R., Yernale N.G., *Bioorg. Med. Chem.*, 2021, **32**:115973 [Crossref], [Google Scholar], [Publisher]
[18]. Zhao J., Zhang Y., Wang M., Liu Q., Lei X., Wu M., Guo S.S., Yi D., Yi D., Li Q., Ma L., Liu Z., Guo F., Wang J., Li X., Wang Y., Cen S., *ACS Infect. Dis.*, 2021, **7**:1535 [Crossref], [Google Scholar], [Publisher]
[19]. Gentile D., Fuochi V., Rescifina A., Furneri P.M., *Int. J. Mol. Sci.*, 2020, **21**:5856 [Crossref], [Google Scholar], [Publisher]
[20]. Dolomanov O.V., Bourhis L.J., Gildea R.J., Howard J.A., Puschmann H., *J. Appl. Crystallogr.*, 2009, **42**:339 [Crossref], [Google Scholar], [Publisher]
[21]. Sheldrick G.M., *Acta Cryst. A*, 2015, **71**:3 [Crossref], [Google Scholar], [Publisher]
[22]. Price G.W., Gould P.S., Marsh A., *J. Chem. Educ.*, 2014, **91**:602 [Crossref], [Google Scholar], [Publisher]
[23]. Rosidi A., Khomsan A., Setiawan B., Riyadi H., Briawan D., *Pak. J. Nutr.*, 2016, **15**:556 [Crossref], [Google Scholar], [Publisher]
[24]. Morris G.M., Huey R., Lindstrom W., Sanner M.F., Belew R.K., Goodsell D.S., Olson A.J., *J. Comput. Chem.,* 2009, **30**:2785 [Crossref], [Google Scholar], [Publisher]
[25]. Suárez D., Díaz N., *J. Chem. Inf. Model.*, 2020, **60**:5815 [Crossref], [Google Scholar], [Publisher]
[26]. Domínguez-Ramírez L., Del Moral-Ramírez E., Cortes-Hernández P., García-Garibay M., Jiménez-Guzmán J., *PLoS One*, 2013, **8**:e79530 [Crossref], [Google Scholar], [Publisher]
[27]. Manoj E., Kurup M.P., Suresh E., *J. Chem. Crystallogr.*, 2008, **38**:157 [Crossref], [Google Scholar], [Publisher]
[28]. Khalid M., Ullah M.A., Adeel M., Khan M.U., Tahir M.N., Braga A.A.C., *J. Saudi Chem. Soc.*, 2019, **23**:546 [Crossref], [Google Scholar], [Publisher]
[29]. Teymourinia H., Salavati-Niasari M., Amiri O., Safardoust-Hojaghan H., *J. Mol. Liq.*, 2017, **242**:447 [Crossref], [Google Scholar], [Publisher]
[30]. Bourhis L.J., Dolomanov O.V., Gildea R.J., Howard J.A., Puschmann H., *Acta Crystallogr. A*, 2015, **71**:59 [Crossref], [Google Scholar], [Publisher]
[31]. Sheldrick G.M., *Acta Crystallogr. C Struct. Chem.*, 2015, **71**:3 [Crossref], [Google Scholar], [Publisher]
[32]. Meng X.Y., Zhang H.X., Mezei M., Cui M., *Curr. Comput. Aided Drug Des.*, 2011, **7**:146 [Crossref], [Google Scholar], [Publisher]
[33]. Zhang G., Zhang A., Meng K., Zhang A., Dong S.Z.Y., *Curr. Org. Chem.*, 2020, **24**:1582 [Crossref], [Google Scholar], [Publisher]
[34]. Overacker R.D., Banerjee S., Neuhaus G.F., Sephton S.M., Herrmann A., Strother J.A., Brack-Werner R., Blakemore P.R., Loesgen S., *Bioorg.*

Med. Chem., 2019, **27**:3595 [Crossref], [Google Scholar], [Publisher]
[35]. De la Guardia C., Stephens D.E., Dang H.T., Quijada M., Larionov O.V., Lleonart R., *Molecules*, 2018, **23**:672 [Crossref], [Google Scholar], [Publisher]
[36]. Jennings M.R., Parks R.J., *Viruses*, 2020, **12**:1242 [Crossref], [Google Scholar], [Publisher]
[37]. Haq I.U., Imran M., Nadeem M., Tufail T., Gondal T.A., Mubarak M.S., *Phytother. Res*., 2021, **35**:680 [Crossref], [Google Scholar], [Publisher]
[38]. Manayi A., Nabavi S.M., Setzer W.N., Jafari S., *Curr. Med. Chem.*, 2018, **25**:4918 [Crossref], [Google Scholar], [Publisher]
[39]. Tang K., Zhang X., Guo Y., *Acta Pharm. Sin. B.*, 2020, **10**:789 [Crossref], [Google Scholar], [Publisher]
[40]. Permpalung N., Thaniyavarn T., Saullo J.L., Arif S., Miller R.A., Reynolds J.M., Alexander B.D., *Transplantation*, 2020, **104**:1280 [Crossref], [Google Scholar], [Publisher]
[41]. Fridriksson B., Bergmann O.M., Olafsson S., *Laeknabladid*, 2017, **103**:125 [Crossref], [Google Scholar], [Publisher]
[42]. Esposito S., N. Principi, *Expert Rev. Respir. Med.*, 2016, **10**:79 [Crossref], [Google Scholar], [Publisher].
[43]. Tagarro A., Cruz-Cañete M., Otheo E., Launes C., Couceiro J.A., Pérez C., Alfayate S., *Anales de Pediatría (English Edition)*, 2019, **90**:317.e1-317.e8 [Crossref], [Google Scholar], [Publisher]
[44]. Shiraki K., Daikoku T., *Pharmacol. Ther.*, 2020, **209**:107512 [Crossref], [Google Scholar], [Publisher]

HOW TO CITE THIS ARTICLE
Ahmed Selmi, Armin Zarei, Wafa Tachoua, Horst Puschmann, Hakimeh Teymourinia, Ali Ramazani. Synthesis and Structural Analysis of a Novel Stable Quinoline Dicarbamic Acid: X-Ray Single Crystal Structure of (2-((4-((2-(Carboxy(methyl)amino)ethoxy)carbonyl) quinoline-2-yl)oxy) ethyl) (methyl)-carbamic Acid and Molecular Docking Assessments to Test Its Inhibitory Potential against SARS-CoV-2 Main Protease. *Chem. Methodol.*, 2022, 6(6) 463-474
https://doi.org/10.22034/CHEMM.2022.335353.1462
URL: http://www.chemmethod.com/article_148534.html